2024 46th Annual International Conference of the IEEE Engineering in Medicine and Biology Society (EMBC) | 979-8-3503-7149-9/24/$31.00 ©2024 IEEE | DOI: 10.1109/EMBC53108.2024.10782349

# A Behavioral Model for Transcutaneous Carbon Dioxide Measurement Using Time-Correlated Single Photon Counting Technique

Isil Isiksalan*, Hakan B. Karli*, Tuna B. Tufan, John Matthews, Bige D. Unluturk, and Ulkuhan Guler

***Abstract*— Millimeter-size carbon dioxide ($CO_2$)-sensitive luminescence films emerge as practical sensors in miniaturized biomedical devices for measuring transcutaneous $CO_2$. The intensity and lifetime of the excited luminophores in the film carry critical information about the $CO_2$ values in the surrounding environment. It has been proven that lifetime-based measurement is superior to intensity-based measurement because of its robustness to confounding factors. Addressing the challenge of accurately determining the rapid nanosecond-scale lifetime of $CO_2$-sensitive luminophores, we introduce a behavioral model using a time-correlated single photon counting system equipped with silicon photomultipliers. We included nonidealities such as dark count rate, afterpulsing, and crosstalk to this model. To recover the lifetime from photon counts, we applied denoising and fitting techniques. With hyperparameter optimization to determine various post-processing parameters, we improved accuracy in recovery for lifetime values ranging from 3 ns to 7 ns. Our results demonstrate the applicability of the proposed model and techniques in real-world scenarios.**

## I. Introduction

With respiratory diseases at the forefront of public health concerns, particularly in the wake of the COVID-19 pandemic, the urgency for advanced diagnostic and monitoring tools for outside clinic use has never been greater [1].

The partial pressure of arterial carbon dioxide ($PaCO_2$) plays a pivotal role in decision making when it comes to chronic respiratory diseases [2]. Elevated $PaCO_2$ levels suggest inadequate ventilation, often seen in advanced respiratory conditions, necessitating interventions including respiratory support. Conversely, low $PaCO_2$ levels indicate excessive ventilation, guiding specific treatment strategies [3]. Thus, $PaCO_2$ measurements are instrumental for tailoring appropriate treatment in chronic respiratory illnesses. This context emphasizes the need for an accurate, noninvasive surrogate measurement method for $PaCO_2$ assessment, i.e., monitoring of transcutaneous carbon dioxide ($PtcCO_2$), which is in direct correlation with the $PaCO_2$ [4].

Transcutaneous monitoring is a noninvasive method of assessing blood gases by measuring the concentration of oxygen and carbon dioxide molecules diffusing through skin [5]. Transcutaneous blood gas monitors typically employ either electrochemical [6] or optical technologies [7], [8], or a combination of these two [9]. Recent optical monitors utilize luminescence sensors to detect $CO_2$ by examining its absorption effects [8], [10]. Measuring the intensity and lifetime of the excited luminophores present in the sensor film provides valuable insights into the molecule concentrations in the surrounding environment, formulated by the Stern-Volmer equation [11]. Notably, the film's luminescent response decays, or 'quenches', in the presence of $CO_2$, enabling accurate measurement of $CO_2$ concentrations [5].

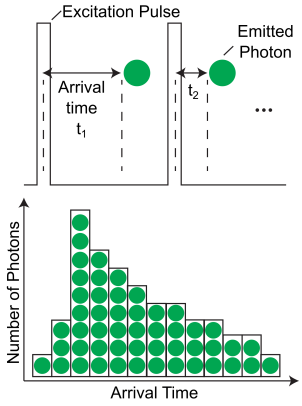


Fig. 1. Principle of time correlated single photon counting [5].

Luminescent measurements fall into two main categories: steady-state and time-resolved. This study focuses on time-resolved luminescence measurement, owing to the advantageous nature of being less susceptible to confounding factors, making it a reliable metric for gauging the efficacy of the measured phenomenon [12]. We specifically investigate the rapid lifetime of $CO_2$-sensitive luminophores, which is $\sim$ 1000 times faster, in the order of a few nanoseconds, compared to oxygen-sensitive luminescence films [13]. This rapid decay presents unique challenges, which our proposed work aims to address by employing the time-correlated single photon counting (TCSPC) technique for its efficiency in quantifying fluorescence lifetime in the time domain. TCSPC involves continuous measurement of fluorescence emissions' timing in relation to synchronized pulsed optical excitation, allowing us to construct a histogram representing the decay of the fluorescence lifetime. The working principle of the TCSPC system is illustrated in Fig. 1.

We investigated the application of a TCSPC system, paired with silicon photomultiplier (SiPM) detectors, for accurately measuring $PtcCO_2$. To achieve this goal, we designed a behavioral model of the system, incorporating various nonidealities, e.g., the SiPM's photon detection efficiency and dark count rate. Then, we employed denoising methods

*These authors contributed equally to this work. I. Isiksalan, T. B. Tufan, J. Matthews and U. Guler are with the Department of Electrical and Computer Engineering, Worcester Polytechnic Institute, Worcester, MA 01609 USA. H. B. Karli and B. Unluturk are with the Department of Electrical and Computer Engineering, Michigan State University, Michigan, MI 48824 USA. This material is based upon work supported in part by the National Science Foundation (NSF) under Grant ECCS-2143898 and in part by the National Health Institute (NIH) under Grant 1R01HL172293-01. Corresponding author: Ulkuhan Guler.

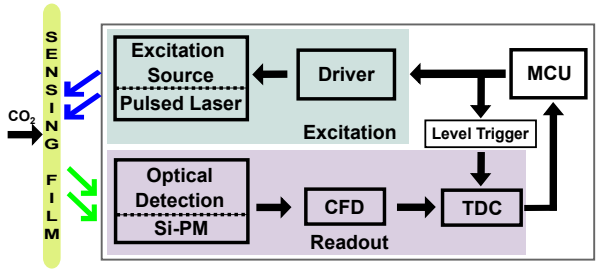


Fig. 2. The block diagram for the behavioral model of the TCSPC setup.

and fitting techniques to extract the rapid lifetime of $CO_2$-sensitive luminophores. To validate our approach, we analyzed the system's performance by calculating errors based on percentage error and successfully determined the original lifetime values with high accuracy.

The organization of this paper is as follows. Section II introduces TCSPC technique, which serves as the foundation for our behavioral model. Section III elaborates on the methodology for the development of the behavioral model, providing a step-by-step explanation of the approach. Following that, Section IV presents our findings, discussing the results obtained from the behavioral model simulations. Finally, in Section V, we provide concluding remarks.

## II. TCSPC System

In this study, the emphasis is placed on a TCSPC system, depicted in Fig. 2, that employs a time-to-digital converter (TDC). The system utilizes a pulsed laser for exciting the sensing film, with silicon photomultipliers (SiPMs) capturing the luminescence response. The full width at half maximum (FWHM) is an important parameter for excitation sources, representing the duration of the laser pulse when its intensity is at half the maximum value. Considering that the FWHM of the excitation source in TCSPC systems should be less than 10% of the lifetime being measured [14], we assumed a pulsed laser with an FWHM well below 300 ps for measuring lifetimes down to 3 ns. This selection allows us to neglect the convolution of the laser's excitation profile with the luminescence response. The system is designed with a 6 µs simulation period for each cycle, one iteration of the excitation pulse, ensuring the capture of all luminophore responses. In the following subsections, we elaborate on the components of the read-out part of the proposed TSCPC system.

### A. Sensing Film

The proposed behavioral model incorporates a model of $CO_2$-sensitive luminescent film based on the physical properties of commercial SPCD1T-D10-YAU-09NaCl sensor (PreSens Precision Sensing). This film, 10 mm in diameter, responds to $CO_2$ levels up to 180 mmHg. When exposed to blue light of 465 nm wavelength, it emits light at two different wavelengths. The $CO_2$-sensitive luminophore peaks at 505 nm, with its emission lifetime decreasing as $CO_2$ levels rise. In contrast, the reference luminophore, which emits light at the wavelength of 600 nm, exhibits an unchanged lifetime despite any variations in the $CO_2$ concentration [10].

To better understand the sensing film, we conducted measurements using a commercial TCSPC device (PicoQuant PicoHarp 300). This allowed us to discover that the reference luminophore has a lifetime of 1 µs, while the $CO_2$-sensitive luminophore exhibits a lifetime of 4 ns under ambient conditions [5]. Additionally, in the worst-case scenario, when the $CO_2$ level in the environment is high, the ratio of initial intensities of the reference and $CO_2$-sensitive luminophores is $\sim$1. We constructed the behavioral model around this ratio to cover the worst-case scenario. The luminescence response characteristic of a single decay event is represented as $I(t) = I_0 \exp\left(-\frac{t}{\tau}\right)$ [11], where $I(t)$ denotes the luminescence intensity, $I_0$ signifies the initial intensity of the luminescent response, $\tau$ shows the lifetime of the luminophore, and $t$ is the time variable.

### B. Optical Detection - SiPMs

SiPMs, consisting of arrays of single-photon avalanche diodes (SPADs), are gaining prominence as optical detection units in TCSPC systems. SiPMs offer a compact size, low voltage requirements, and robustness alongside high gain and stability [15]. SPADs are highly sensitive and provide precise photon arrival times, yet they have an inherent dead time during which no detection can occur. This issue is elegantly addressed in SiPMs where multiple SPADs are connected in parallel, enhancing the dynamic range and photon counting rates [16]. We have chosen the Hamamatsu MPPC S13360-1375PE for the SiPM model.

We assumed operation at room temperature and utilized values for key parameters from the datasheet to integrate this detector into the proposed model. Among these parameters, the photon detection efficiency (PDE) is a critical performance metric, reflecting the probability that an incident photon will produce a detectable signal. PDE is inherently wavelength-dependent, and the SiPM's ability to detect photons varies across different wavelengths. For our sensing film, which contains two luminophores with peak emission at 600 nm for the reference and 505 nm for $CO_2$ sensitivity, it is essential to consider these wavelength-specific PDE values. According to the datasheet, the PDE at 600 nm is 33%, and at 505 nm, it is 47%.

We also accounted for the dark count rate (DCR), which represents the intrinsic noise signals in SiPMs caused by the thermal generation of carriers within the silicon bandgap. These spurious signals, which occur even in the absence of photon excitation [17], can adversely affect the detector's performance by increasing the noise baseline [18]. If this event occurs, it is indistinguishable from a real photon event and is added to the photon histogram. According to the datasheet, the typical DCR for the chosen SiPMs is 90 kilo count per seconds (kcps). Following the same approach in the literature [18], the DCR is modeled using a Poisson distribution to represent the statistical occurrence of dark counts over time, with the mean generation time, $t_{cg}$, inversely proportional to the DCR.

The proposed model also considers crosstalk in SiPMs, where photon emissions from one SPAD can trigger

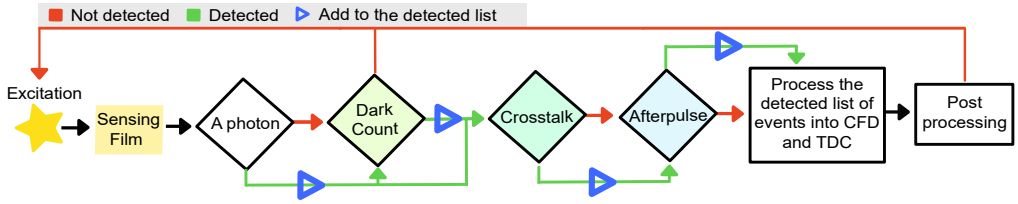


Fig. 3. Process flowchart illustrating the integration of system nonidealities.

avalanches in neighboring SPADs [19]. The chosen SiPM has a 7% crosstalk probability at room temperature with the recommended overdrive voltage. To accurately model crosstalk, its timing is evaluated in relation to the SiPM output pulse's rise time. For crosstalk events within the output pulse's rise time, pulse timing adjustments are made to accurately reflect the timing changes these events introduce. This is simulated by applying a Gaussian time shift to each detected photon event, with a standard deviation set to one-third of the maximum shift of 1 ns, according to the datasheet of the chosen model.

In SiPM-based TCSPC systems, afterpulsing occurs when charge carriers, previously trapped within the SPADs, are spontaneously released, leading to additional, false photon detection events [20]. These afterpulses usually emerge within 6 ns to 10 ns following the primary photon [19], with the possibility of affecting the rise time of the signal by picoseconds to nanoseconds. To capture this effect, we introduce a mechanism for afterpulsing based on the probability density function of afterpulse time point [19].

### C. Constant Fraction Discriminator

The output pulses from SiPMs are quite unstable. Due to the random amplification mechanism in the detectors, the single-photon pulses exhibit significant amplitude jitter [21]. Consequently, a simple leading-edge discriminator is unsuitable for triggering such pulses, as the amplitude jitter would result in a timing jitter comparable to the pulse's rise time. Therefore, we implement a constant-fraction discriminator (CFD) at the detector output. CFDs trigger at a consistent fraction of the pulse amplitude, effectively mitigating timing jitter induced by pulse height variations. Additionally, CFDs incorporate a discriminator that filters out input pulses below a selectable threshold, allowing us to disregard environmental noise or minor background pulses from the detector [21].

In TCSPC systems, passing the photon pulses from the detector through a CFD after initial detection is common practice. The output pulses from the CFD have a constant width and timing that is independent of the amplitude of the detector pulses [21]. Although CFDs introduce a constant propagation delay and minimal timing jitter, we assume a propagation delay of 1 ns for a 20% fraction according to $t_d \approx (1 - f)$, where $f$ is the fraction of the peak amplitude, and $t_d$ is the total delay. Furthermore, based on the datasheet, we have conservatively added a timing jitter of 20 ps.

### D. Time-to-Digital Converter

In our TCSPC system, the TDC is pivotal for measuring the interval between photon excitation and detection by the SiPM, aiding in histogram construction. Our selected TDC model, the TDC7201 from Texas Instruments, offers a resolution of 55 ps, aligning with our precision requirements. Moreover, to address the clock jitter from the ring oscillator, we model it as a Gaussian jitter, aligning with methodologies from [22], [23] on oscillator jitter. This method effectively incorporates timing variability into our analysis.

## III. Methodology

This section presents the behavioral model's flow and describes the post-processing stream that reconstructs the decay of $CO_2$-sensitive luminophores to determine lifetime information.

### A. Behavioral Model Development

Fig. 3 depicts a flowchart presenting a comprehensive overview of the behavioral model's process flow. The process begins with the 'Excitation' phase, after which the sensing film emits photons when exposed to light. The system evaluates the PDE of the SiPM, taking into account the specific PDE values associated with each luminophore present in the sensing film. Based on these probabilities, if a genuine photon is detected, its timestamp is added to a 'detected list' of events, as noted in Fig. 3.

Irrespective of photon detection, the model determines the likelihood of a dark count using the DCR specified in the datasheet, simulating a Poisson distribution for the selected SiPM [18]. Any identified dark counts are added to the list. If no photon or dark count is detected, the sequence is restarted.

Then, the model checks for crosstalk. If crosstalk is detected, it can slightly increase the output signal amplitude of the SiPM, potentially causing changes to the signal's rise time. It is simulated as an individual event closely following real photon or dark count events to model its impact. The model also considers afterpulsing events, which can occur following an avalanche caused by a photon or a dark count, and includes them in the detected list if they occur.

Events on the detected list for each cycle are then processed through the CFD, which effectively filters out most afterpulses by eliminating lower amplitude events that do not significantly alter the signal's rising edge. The TDC further refines the detected list, which now includes timestamps that have passed the CFD, by imposing a Gaussian timing jitter on the timestamps of the rising edge. Once each cycle is complete, the TDC output array is set for post-processing.

### B. Histogramming and Post-processing

Upon obtaining the TDC output array, which includes timestamps with system-induced errors, the data is trans-

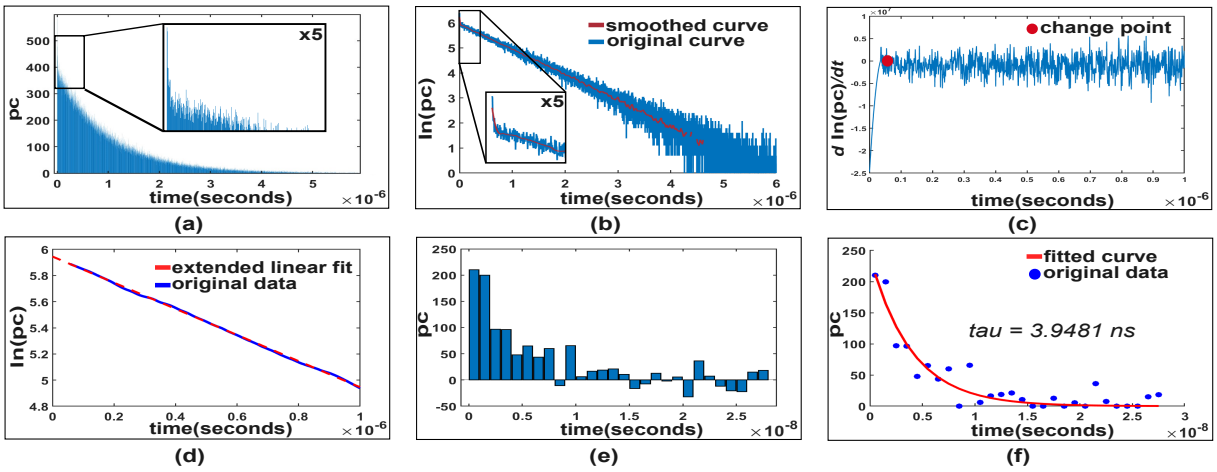


Fig. 4. (a) The TDC output histogram for pc (photon counts) of 800,000 cycles, (b) logarithmic transformation and smoothing of TDC histogram, inset: x5 magnification, (c) derivative of the In(photons) graph constructed to find the change point, (d) linear regression on smoothed logarithmic data with extension to t=0, (e) identification of $CO_2$-sensitive data points, and (f) characteristic lifetime ($\tau$) estimation through exponential decay curve fitting.

formed into a histogram with a time bin width of 1 ns, inline with the TDC's modeled resolution of 55 ps. The histogram, as illustrated in Fig. 4a, reveals two overlapping luminescence decays; one associated with the reference luminophores, and the other with $CO_2$-sensitive luminophores, where the reference decay exhibits a notably longer lifetime. Fig. 4a inset highlights the transition from the combined luminescent responses to the solely reference response.

Differentiation between these two responses is achieved by identifying the transition point in the histogram. This involves converting the histogram into a curve and applying a Savitzky-Golay filter [24]. The window size for this smoothing filter is determined through hyperparameter optimization, systematically finding the most effective parameter values. The comparison of unsmoothed and smoothed curves of the natural logarithm of photon counts is depicted in Fig. 4b.

Subsequently, the derivative of the logarithmic curve is calculated to identify the change point, as shown in Fig. 4c. This point signifies a transition in the curve's behavior, indicating the completion of the $CO_2$-sensitive luminophore's decay. Counts before this transition are influenced by both reference and $CO_2$-sensitive luminophores, whereas counts after solely reflect the reference luminophore's response.

Due to noise in the histogram, we faced challenges in precisely identifying the change point in Fig. 4b. Therefore, while dividing the data into 2 segments, we put a gap interval around the change point that is not included in either segment. This interval is determined by two parameters, which are identified through hyperparameter optimization and are on the ns scale, since we quantized the time of the histogram bins to 1 ns. The first is the *ref_shift*, the time shift between the change point and the cut-off point of combined photon counts. The second is the *sens_shift*, the time shift between the change point and the starting point of reference photon counts.

Once the gap interval was set, we focused on the segment representing only the reference luminophores, and additional smoothing and linear fitting were applied to the logarithmically scaled data as seen in Fig. 4d. The y-intercept obtained from this fitting provided us with the initial intensity of the reference luminophores. With the known lifetime ($\tau_{ref}$) of the reference luminophores, we reconstructed their contribution and subtracted it. This subtraction yielded a histogram that only showed $CO_2$-sensitive luminophore photon counts as illustrated in Fig. 4e.

To determine the lifetime, we applied exponential fitting, with a focus on early-time photon counts, which were weighted more significantly. The number of early samples that are weighted more heavily and the corresponding weights are refined via hyperparameter optimization. Finally, the accuracy of this fitting was evaluated using percentage error analysis. The resulting fitting curve and extracted lifetime for a lifetime of 4 ns are illustrated in Fig. 4f, demonstrating the effectiveness of the proposed methodology in capturing the decay characteristics of the luminophore.

## IV. Results and Discussion

After building the behavioral model and the lifetime estimation algorithm for $CO_2$-sensitive luminophores, we tested it for a range of rapid lifetime values which vary from 3 ns to 7 ns, imitating a real-case scenario. We employed the hyperparameter optimization toolbox for a detailed examination of several key parameters, as defined in Section III: i) identifying the optimal window size for both smoothing processes, ii) determining the most effective ranges for change point detection to accurately capture transition points, and iii) calibrating the weights and number of weighted samples for the $CO_2$-sensitive curve fitting for varying cycle counts. Investigating these parameters' optimal values in post-processing significantly contributed to the method's accuracy in recovering lifetime values.

We generated five datasets per cycle count for each $\tau$ value, focusing on minimizing the percentage error in estimating the true lifetime values, maintaining accuracy above 85% across different scenarios. This hyperparameter optimization process led to best-fit post-processing parameters, effective across various cycle counts, showcased in Table I.

TABLE I

HYPERPARAMETER OPTIMIZATION PARAMETERS

| Cycle Count | Window to Signal Size Ratio (%) | Ref_shift / Sens_shift (ns) | Weight/# of Weighted Samples | Accuracy (%) |
|---|---|---|---|---|
| 200,000 | 6.75 / 3.64 | 25 / 6 | 2 / 2 | 86.18 |
| 400,000 | 2.20 / 9.46 | 26 / 0 | 1 / 2 | 89.59 |
| 600,000 | 1.13 / 4.94 | 27 / 13 | 5 / 1 | 90.98 |
| 800,000 | 1.20 / 9.57 | 27 / 3 | 4 / 1 | 90.82 |
| 1,000,000 | 1.30 / 9.96 | 3 / 14 | 4 / 1 | 89.97 |

After the determination of post-processing parameters, we reevaluated internal parameters, including cycle count, one of the design parameters for future hardware system implementation. In the TCSPC system, one iteration in the process, corresponding to the duration between excitation pulses, was established as $6\mu$s. In each cycle, the system captures a maximum of one photon due to pixel pitch and the PDE of SiPMs, a limitation common to most TCSPC systems requiring multiple successive excitations to construct a better histogram [25]. To acquire the lifetime value of fast-decaying $CO_2$-sensitive luminophores through post-processing, we required a minimum of 200,000 cycles, corresponding to 1.2 seconds, to accumulate the necessary histogram counts before post-processing. While photobleaching is not a concern with the TCSPC method for lifetime measurements [12], prioritizing the reduction of the sensing film's exposure to excitation pulses and minimizing power consumption is a key consideration which requires limiting the cycle count.

According to Table I, it was observed that higher cycle counts could improve accuracy up to a certain point. Beyond this point, increasing cycle count came with the cost of increased DCR which eventually drove the accuracy down. As a result, we identified a cycle count of 600,000 as the highest accuracy while effectively managing DCR. At this cycle count, the accuracy of retrieving the lifetime value reached 90.98% as seen in Table I. A cycle count of 400,000 would provide slightly lower accuracy while reducing the power consumption by one-third.

## V. CONCLUSION

This paper presents a comprehensive behavioral model for transcutaneous carbon dioxide measurement using a TCSPC system with SiPM detectors, highlighting the potential for future system miniaturization and efficiency improvements through the integration of CMOS SPAD arrays and on-chip histogramming. By optimizing post-processing parameters, we achieved an accuracy of 90.98% in the lifetime measurement of $CO_2$-sensitive luminophores at a 600,000 cycle count, while accounting for system nonidealities. Our findings advocate for the preliminary behavioral modeling of TCSPC systems to evaluate the performance of various components to be selected for future design. This methodology not only advances our understanding of TCSPC in luminescent sensing but also opens new doors for noninvasive medical monitoring technologies, promising innovative applications in healthcare.


## ACKNOWLEDGMENT

We would like to express our sincere appreciation to Panagiotis Traganitis, Ph.D., for his expert guidance and invaluable support throughout this research.


## REFERENCES


[1] U. Guler *et al.*, "Emerging Blood Gas Monitors: How They Can Help With COVID-19," *IEEE Solid-State Circuits Magazine*, vol. 12, no. 4, 2020.

[2] P. S. M. Z. M. Castro, D. and M. Keenaghan, "Arterial blood gas," in *StatPearls*. Treasure Island (FL): StatPearls Publishing, 2024.

[3] I. Costanzo *et al.*, "Respiratory monitoring: Current state of the art and future roads," *IEEE Reviews in Biomedical Engineering*, vol. 15, pp. 103–121, 2022.

[4] M. Dicembrino *et al.*, "End-tidal CO2 and transcutaneous CO2: Are we ready to replace arterial CO2 in awake children?" *Pediatric Pulmonology*, vol. 56, no. 2, 2021.

[5] T. B. Tufan and U. Guler, "A transcutaneous carbon dioxide monitor based on time-domain dual lifetime referencing," *IEEE Transactions on Biomedical Circuits and Systems*, 2023.

[6] J. W. Severinghaus and A. F. Bradley, "Electrodes for blood po2 and pco2 determination," *Journal of applied physiology*, vol. 13, no. 3, pp. 515–520, 1958.

[7] V. V. Tipparaju *et al.*, "Wearable transcutaneous co monitor based on miniaturized nondispersive infrared sensor," *IEEE sensors journal*, vol. 21, no. 15, pp. 17 327–17 334, 2021.

[8] T. Tufan and U. Guler, "A fluorescent thin film-based miniaturized transcutaneous carbon dioxide monitor," in *Proc. IEEE Biomed. Circuits Syst. Conf.*, 2021, pp. 1–5.

[9] J. W. Severinghaus, "A combined transcutaneous po2-pco2 electrode with electrochemical hco3-stabilization," *Journal of Applied Physiology*, vol. 51, no. 4, pp. 1027–1032, 1981.

[10] T. B. Tufan and U. Guler, "A miniaturized transcutaneous carbon dioxide monitor based on dual lifetime referencing," in *2022 IEEE Biomedical Circuits and Systems Conference (BioCAS)*, Oct. 2022, pp. 144–148.

[11] J. R. Lakowicz, Ed., *Time-Domain Lifetime Measurements*. Boston, MA: Springer US, 2006, pp. 97–155.

[12] M. Y. Berezin and S. Achilefu, "Fluorescence lifetime measurements and biological imaging," *Chemical reviews*, vol. 110, no. 5, pp. 2641–2684, 2010.

[13] T. B. Tufan *et al.*, "Implementation techniques for transcutaneous carbon dioxide monitoring: Approaches for wearable smart health applications," *IEEE Transactions on Biomedical Engineering*, 2023.

[14] M. Wahl, "Time-correlated single photon counting," 2009.

[15] H.-M. Tsai *et al.*, "Rapid measurement of fluorescence lifetimes using sipm detection and waveform sampling," in *2016 IEEE Nuclear Science Symposium, Medical Imaging Conference and Room-Temperature Semiconductor Detector Workshop (NSS/MIC/RTSD)*, 2016, pp. 1–3.

[16] M. Perenzoni, "Single-photon avalanche diode-based detection and imaging: Bringing the photodiode out of its comfort zone," *IEEE Solid-State Circuits Magazine*, vol. 10, no. 3, pp. 26–34, 2018.

[17] S. Gundacker and A. Heering, "The silicon photomultiplier: fundamentals and applications of a modern solid-state photon detector," *Physics in Medicine & Biology*, vol. 65, no. 17, p. 17TR01, 2020.

[18] W.-J. Yu *et al.*, "Dark count in single-photon avalanche diodes:a novel statistical behavioral model," *Chinese Physics B*, vol. 29, 04 2020.

[19] J. Rosado and S. Hidalgo, "Characterization and modeling of crosstalk and afterpulsing in hamamatsu silicon photomultipliers," *Journal of Instrumentation*, vol. 10, no. 10, p. P10031–P10031, Oct. 2015.

[20] C. Wang *et al.*, "Afterpulsing effects in spad-based photon-counting communication system," *Optics Communications*, vol. 443, pp. 202–210, 2019.

[21] W. Becker, *The bh TCSPC handbook. 10th edition*. Becker Hickl GmbH, 2023.

[22] J. A. McNeill and D. S. Ricketts, *Designer's Guide to Jitter in Ring Oscillators*. Springer, 2009.

[23] U. Güler and G. Dündar, "Modeling cmos ring oscillator performance as a randomness source," *IEEE Transactions on Circuits and Systems I: Regular Papers*, vol. 61, no. 3, pp. 712–724, 2014.

[24] R. W. Schafer, "What is a savitzky-golay filter? [lecture notes]," *IEEE Signal Processing Magazine*, vol. 28, no. 4, pp. 111–117, 2011.

[25] W.Becker, Ed., *Overview of Photon Counting Techniques*. Springer, 2005, pp. 11–24.